Environmental Science & Technology

pubs.acs.org/est Article

Transformation of Highly Stable Pt Single Sites on Defect Engineered Ceria into Robust Pt Clusters for Vehicle Emission Control

Wei Tan, Shaohua Xie, Yandi Cai, Meiyu Wang, Shuohan Yu, Ke-Bin Low, Yuejin Li, Lu Ma, Steven N. Ehrlich, Fei Gao,* Lin Dong, and Fudong Liu*

Cite This: *Environ. Sci. Technol.* 2021, 55, 12607−12618 Read Online

ACCESS | Metrics & More | Article Recommendations | Supporting Information

ABSTRACT: Engineering surface defects on metal oxide supports could help promote the dispersion of active sites and catalytic performance of supported catalysts. Herein, a strategy of ZrO_2 doping was proposed to create rich surface defects on CeO_2 (CZO) and, with these defects, to improve Pt dispersion and enhance its affinity as single sites to the CZO support (Pt/CZO). The strongly anchored Pt single sites on CZO support were initially not efficient for catalytic oxidation of CO/C_3H_6. However, after a simple activation by H_2 reduction, the catalytic oxidation performance over Pt/CZO catalyst was significantly boosted and better than Pt/CeO_2. Pt/CZO catalyst also exhibited much higher thermal stability. The structural evolution of Pt active sites by H_2 treatment was systematically investigated on aged Pt/CZO and Pt/CeO_2 catalysts. With H_2 reduction, ionic Pt single sites were transformed into active Pt clusters. Much smaller Pt clusters were created on CZO (*ca.* 1.2 nm) than on CeO_2 (*ca.* 1.8 nm) due to stronger Pt-CeO_2 interaction on aged Pt/CZO. Consequently, more exposed active Pt sites were obtained on the smaller clusters surrounded by more oxygen defects and Ce^{3+} species, which directly translated to the higher catalytic oxidation performance of activated Pt/CZO catalyst in vehicle emission control applications.

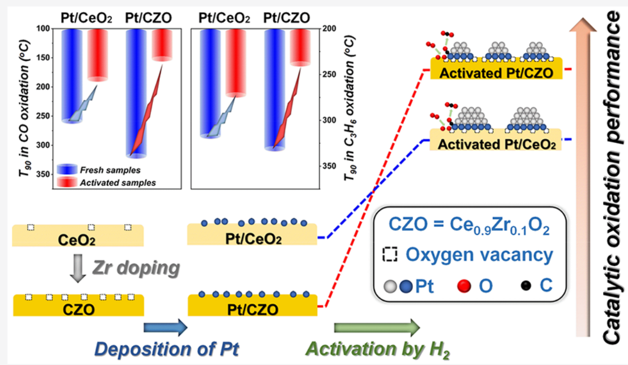

KEYWORDS: *engineering surface defects, Pt single sites, structural evolution, activation treatment, catalytic oxidation reactions*

1. INTRODUCTION

To meet the increasingly more stringent automotive emission standards, it is imperative to develop more efficient catalysts that can better utilize precious metals especially after aging.[1] Platinum group metals (PGMs), such as Pt, Pd, and Rh, supported on various refractory metal oxides have been widely investigated as emission control catalysts, among which Pt-based catalysts have attracted much attention due to their excellent activity for carbon monoxide (CO) and hydrocarbon (HC) oxidation. Perhaps, another reason for the abundance of Pt-related work is because of its relatively low price relative to Pd and Rh in recent years.[2,3] In addition to choosing the optimal PGMs with different sizes or shapes as active sites, designing catalyst supports with tunable physical−chemical properties can also lead to optimized state of PGM and thus improved catalytic performance and stability. In this regard, engineering surface defects on widely used metal oxide supports is both academically interesting and industrially useful. For example, defect-engineered TiO_2 has been reported as an efficient photocatalytic material for various reactions, with the fine-tuned TiO_2 exhibiting enhanced visible light response.[4,5] The surface defects on TiO_2 could help disperse and stabilize PGMs and tune the electronic states, thus adjusting their catalytic performance.[6−10] This approach has also been widely applied to ZnO, Co_3O_4, and Nb_2O_5 for CO/HCs oxidation reactions.[11−15] The surface defects on these metal oxides were found to enhance the interaction between PGMs and supports, to facilitate the adsorption, activation, and transfer of active oxygen, and thus to promote the catalytic oxidation performance.

CeO_2 is a commonly used support and an important component of oxygen storage materials in automotive exhaust control catalysts due to its facile redox ability and oxygen mobility. Much effort has been devoted to exploiting the potential of Pt-CeO_2-based catalysts for practical applications in vehicle emission controls, aiming to meet the requirements for both low-temperature catalytic activity and high-temper-

Received: May 5, 2021
Revised: August 29, 2021
Accepted: August 30, 2021
Published: September 8, 2021

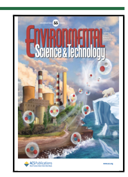

https://doi.org/10.1021/acs.est.1c02853
Environ. Sci. Technol. 2021, 55, 12607−12618

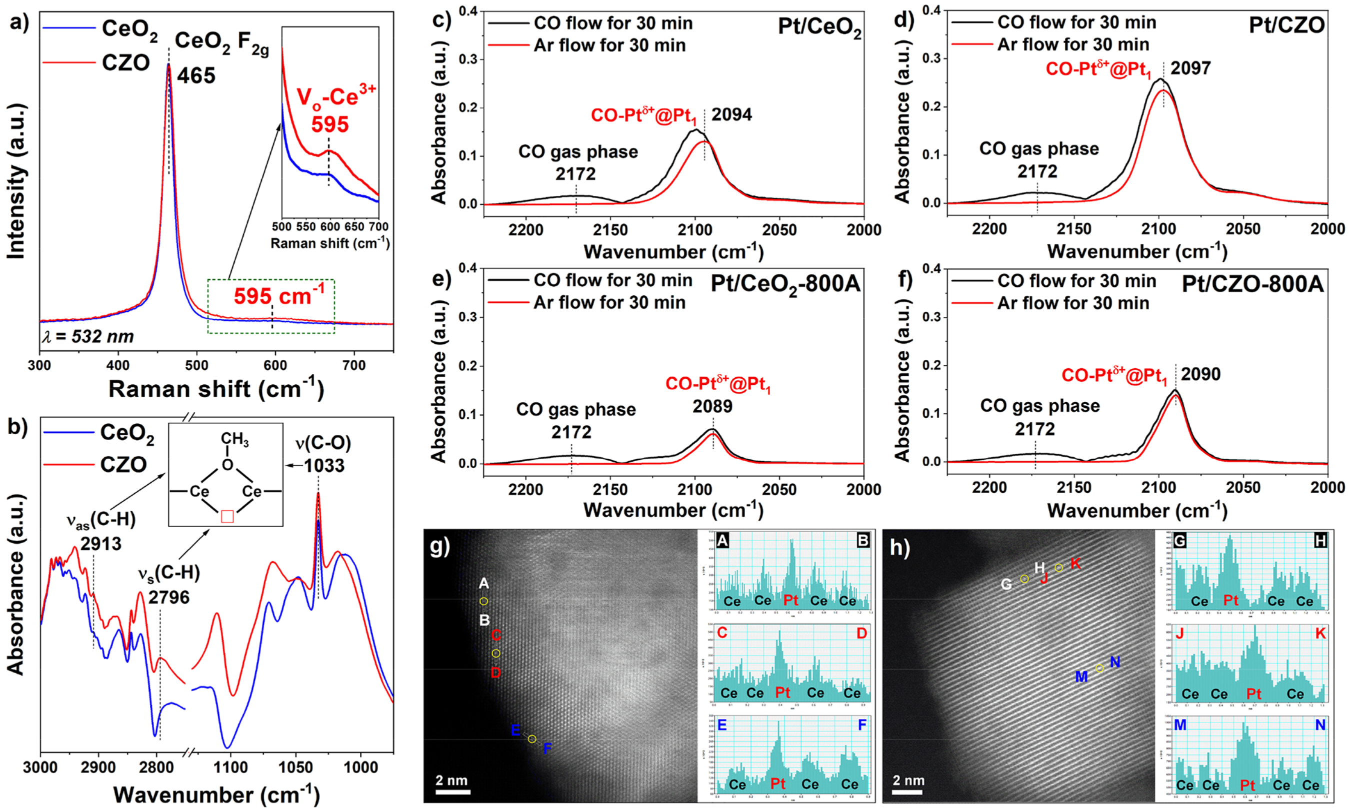

Figure 1. (a) Raman spectra of CeO_2 and CZO; (b) *in situ* DRIFTS of methanol adsorption on CeO_2 and CZO at 25 °C; *in situ* DRIFTS of CO adsorption at 50 °C on (c) Pt/CeO_2, (d) Pt/CZO, (e) Pt/CeO_2-800A, and (f) Pt/CZO-800A; HAADF-STEM images and line profiles of (g) Pt/CeO_2-800A and h) Pt/CZO-800A. Note: Some of the Ce atoms marked in the line profiles of Pt/CZO-800A could be Zr atoms.

ature thermal stability. Recently, there have been vigorous and continuous discussions on developing efficient Pt ensemble/cluster catalysts from Pt single-atom catalysts (SACs) supported on CeO_2-based materials.[16−18] Although the Pt SACs highly stabilized by CeO_2 may not be efficient catalysts for CO/HCs oxidation, after appropriate activation treatment (e.g., steam aging, CO/H_2/HC reduction), the catalytic performance of Pt single sites could be substantially promoted.[18−22]

In addition to the promotion effect of activation treatment, the initial states of Pt single sites also had a significant impact on the catalytic performance of the subsequently activated Pt/CeO_2 catalysts. For instance, it was reported that the strongly anchored Pt single sites on CeO_2 prepared by the atom trapping strategy, which had limited initial CO oxidation activity, could be transformed into highly efficient Pt clusters after appropriate reduction treatment with CO, while the counterpart catalyst prepared by strong electrostatic adsorption (SEA) method with relatively weak Pt-CeO_2 interaction showed inferior catalytic oxidation performance after the same activation procedure.[16] To prepare strongly anchored Pt single sites on CeO_2, surface defect engineering on CeO_2-based supports was one of the general methods used to create more surface defects and Ce^{3+} species for Pt single site anchoring.[17,23−28] The reaction between Ce^{3+} species and PtO_2 ($2Ce^{3+} + PtO_2 \rightarrow Ce^{4+}–O–Pt^{2+}–O–Ce^{4+}$) was proposed to be responsible for the formation of strong Pt−O−Ce bonds, promoting the dispersion and stabilization of Pt single sites.[28,29] However, so far, the commonly used methods for creating surface defects on CeO_2-based supports, such as reducing CeO_2 using various reactants/plasma irradiation and controlling the particle size of CeO_2,[25,26,28,30] are complex and may not be viable for commercial applications. Therefore, it is necessary to develop facile and cost-effective strategies to engineer the surface defects of CeO_2-based supports for the easy fabrication of strongly anchored Pt single sites and the transformation of such single sites into highly active catalytic centers for targeted reactions.

Doping CeO_2 with different transition metals or rare-earth elements (e.g., Cu, Zr, La, Y, Pr, *etc.*) has been recognized as an efficient method to fine-tune CeO_2 in terms of specific surface area, thermal stability, and oxygen mobility.[31−35] Catalysts supported on doped CeO_2 materials exhibit more superior catalytic performance than those supported on pristine CeO_2.[32,36−43] In the field of automotive emission control, Zr is one of the most commonly used elements to modify the physical−chemical properties of CeO_2.[31,44,45] Incorporating Zr into CeO_2 can improve its hydrothermal stability and redox capacity, and, due to the smaller ion radius of Zr^{4+} comparing to Ce^{4+}, the resulting lattice distortion also can increase the density of surface defects and Ce^{3+} species on Zr doped CeO_2.[46] Comparing to previously reported methods, Zr doping is undoubtedly more convenient and cost-effective in defect engineering of CeO_2-based materials. Although CeO_2−ZrO_2 solid solutions have been widely used in vehicle emission control catalysts,[47−50] no systematic work has been reported focusing on the impact of defect engineering by Zr doping into CeO_2 on the state of supported Pt single sites. Furthermore, the structural evolution of Pt single sites during the activation process is also worth exploring to better understand the nature of catalytically active centers for the reactions of interest.

https://doi.org/10.1021/acs.est.1c02853
Environ. Sci. Technol. 2021, 55, 12607−12618

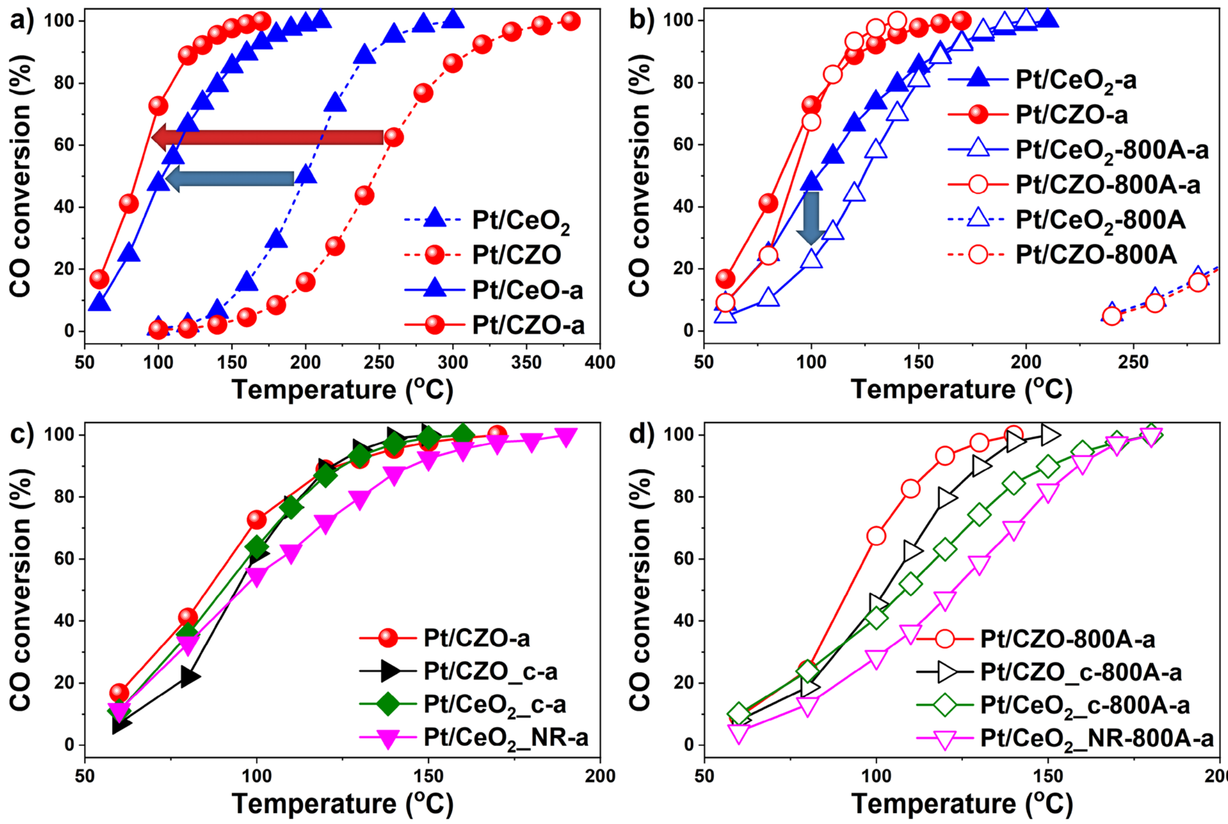

Figure 2. CO oxidation activities on (a) fresh and (b) aged catalysts that were pretreated with air at 300 °C or activated with 10% H_2 at 400 °C; CO oxidation activities on (c) fresh and (d) aged Pt catalysts supported on CeO_2 nanorod (CeO_2_NR), commercial CeO_2 (CeO_2_c) and commercial $CeZrO_x$ (CZO_c) that were activated by 10% H_2 at 400 °C. (Reaction condition: [CO] = 1%, [O_2] = 1%, Ar balance, with a weight hourly space velocity (WHSV) of 200 000 mL·$g_{cat.}^{-1}$·h^{-1}).

In this study, a facile defect engineering strategy for CeO_2 by Zr doping has been successfully developed. Increased surface defect density and Ce^{3+} concentration have been achieved on the engineered CeO_2 support. Such defect engineered support was highly beneficial for anchoring Pt species as single sites upon simple impregnation because of the stronger interaction between Pt and CeO_2 comparing to the pristine CeO_2 support. Upon a simple reductive activation by H_2, the strongly anchored Pt single sites on Zr-doped CeO_2 were transformed into highly active Pt clusters, outperforming the state-of-the-art Pt/CeO_2 catalyst for CO and C_3H_6 oxidation. The impact of Zr doping on the microstructure and catalytic oxidation performance of Pt-CeO_2-based catalyst was systematically investigated using a series of characterization techniques, which revealed a detailed process of structural transformation of Pt single sites into robust Pt clusters under reduction atmosphere. The structure–activity relationship for the Pt catalyst supported on defect-engineered CeO_2 support was also established accordingly.

2. MATERIALS AND EXPERIMENTAL METHODS

Pt catalysts used in this work were supported on CeO_2 and $Ce_{0.9}Zr_{0.1}O_2$. The supports were prepared by (co)precipitation method.[S1] 1 wt % Pt ($Pt(NH_3)_4(NO_3)_2$ as precursor) was loaded on CeO_2 and $Ce_{0.9}Zr_{0.1}O_2$ (Pt/CeO_2 and Pt/CZO) using incipient wetness impregnation (IWI) method. To study the thermal stability, the prepared catalysts were also aged at 800 or 1000 °C for 12 h in air, denoted with "-800A" or "-1000A" suffix, respectively. Before CO oxidation activity test, the samples were pretreated with flowing air at 300 °C or activated with 10% H_2/Ar at 400 °C for 1 h. Before C_3H_6 oxidation activity test, the activation treatment with 10% H_2/Ar was performed at 500 °C for 1 h. The activated samples were denoted with "-a" (-a = after activation by H_2 reduction).

Details of catalyst preparation, catalytic activity testing and characterizations are described in Supporting Information (SI) Text S1, Text S2, and Text S3.

3. RESULTS AND DISCUSSION

3.1. Surface Defects and Pt Single Sites. As reported elsewhere, the surface defects on CeO_2 could significantly contribute to the formation and stabilization of Pt single sites.[23] Herein, to prepare a highly dispersed Pt single site catalyst, Zr doping was applied to create more surface defects on CeO_2 support. XRD patterns of CeO_2 and CZO are shown in SI Figure S1, from which only diffraction peaks assigned to cubic fluorite CeO_2 could be found, suggesting that Zr was successfully doped into CeO_2 matrix without forming crystalline ZrO_2. The CZO support showed lower diffraction peak intensity and smaller crystal size than pristine CeO_2 support (SI Table S1). The deposition of Pt onto CeO_2 and CZO followed by 550 °C calcination resulted in increased intensity of the CeO_2 diffraction peaks, but after aging treatment at 800 °C, no appreciable change was observed. As illustrated by the EDS mapping images of Pt/CZO-800A (SI Figure S2), ZrO_2 was found to be uniformly distributed in CeO_2, further supporting the formation of a homogeneous CeO_2−ZrO_2 mixed oxide. The normalized Raman spectra of

CeO_2 and CZO are illustrated in Figure 1a. The intensive band at 465 cm^{-1} is attributed to the triply degenerated F_{2g} mode of fluorite-type CeO_2. The band at 595 cm^{-1} is ascribed to the defect-induced mode, related to the formation of oxygen vacancies in CeO_2.[46,52] The increased intensity of the band at 595 cm^{-1} for CZO indicates that higher concentration of surface defects was obtained through Zr doping into CeO_2. To further verify this viewpoint, *in situ* DRIFTS of methanol adsorption was conducted on CeO_2 and CZO at 25 °C (Figure 1b). The bands at 1033, 2796, and 2913 cm^{-1} can be assigned to bridging methoxy species, with the bridged Ce ions having an oxygen vacancy in the neighborhood.[53] These three bands on CZO were more intensive than those on CeO_2, indicating that more surface oxygen vacancies were indeed formed on CZO support.

After Pt deposition, no crystalline Pt or PtO_x was detected by XRD (SI Figure S1), suggesting that Pt is highly dispersed on both CeO_2 and CZO, probably in single site form. To verify this, *in situ* DRIFTS of CO adsorption was performed on Pt/CeO_2 and Pt/CZO (Figure 1c,d). Under the CO flow, a well-defined band at *ca.* 2095 cm^{-1} and a broad band at *ca.* 2172 cm^{-1} could be observed on both samples, which can be assigned to CO adsorbed on Pt single sites (CO-$Pt^{\delta+}$@Pt_1) and gas phase CO, respectively.[54−56] After Ar purge, only the band at 2095 cm^{-1} remained, suggesting that the CO species adsorbed on Pt single sites is very stable.[57] It is noteworthy that the intensity of the CO adsorption band on Pt/CZO was much more intense than that on Pt/CeO_2 (SI Table S2), indicating a higher exposure of Pt species on CZO support. For a vehicle emission control catalyst, high thermal stability is greatly required. Therefore, *in situ* DRIFTS of CO adsorption was also conducted on aged samples, that is, Pt/CeO_2-800A and Pt/CZO-800A (Figure 1e,f). After CO adsorption and Ar purge, similar to what was observed on the fresh samples, only the CO adsorbed species on Pt single sites could be observed on the aged samples. The decrease in the intensity of CO-$Pt^{\delta+}$@Pt_1 bands and the shift of these bands to lower wavenumbers could be due to the migration of Pt single site into CeO_2 or CZO lattice.[58] However, the Pt/CZO-800A still showed much higher Pt site exposure than the Pt/CeO_2-800A counterpart.

The HAADF-STEM images of Pt/CeO_2-800A and Pt/CZO-800A are shown in Figure 1g,h and SI Figure S3. In consistence with the *in situ* DRIFTS results of CO adsorption, no identifiable Pt clusters or nanoparticles were found on Pt/CeO_2-800A and Pt/CZO-800A. With the aid of elemental line profiling, isolated bright dots on the supports could be identified as Pt single sites. Interestingly, for Pt/CeO_2-800A, most of the Pt single sites were located at the step edges of CeO_2 particles, while for Pt/CZO-800A, Pt single sites were widely distributed on both step edges and Ce atom columns within surface lattice. These results clearly show that, as expected, Zr doping into CeO_2 indeed created more surface defects, which could act as additional anchoring sites for atomically dispersed Pt species. Given the comparable specific surface areas for CeO_2 (44 m^2/g) and CZO (59 m^2/g) supports (SI Table S3) and their similar morphology, the higher density of surface defects on CZO should be the main reason for the much higher Pt exposure on Pt/CZO and Pt/CZO-800A samples.

3.2. Catalytic Performance for CO Oxidation. CO oxidation is a key reaction in vehicle emission control and was selected as a probe reaction to evaluate the catalytic performance of Pt/CeO_2 and Pt/CZO catalysts. As shown in Figure 2a, before activation, both Pt/CeO_2 and Pt/CZO exhibited limited CO oxidation activity, which should be resulted from the CO poisoning effect where CO was overstrongly bound to Pt single sites.[16] It has to be noted that the Pt single sites supported on CZO even exhibited inferior CO oxidation activity comparing to those supported on CeO_2 probably due to the over-rigid local coordination structure of Pt/CZO with stronger Pt-CeO_2 interaction. However, after activation by H_2 reduction, the CO oxidation activity on Pt/CZO-a showed significant enhancement, with a T_{90} (temperature required to achieve 90% CO conversion) of 120 °C, much lower than that on Pt/CeO_2-a (T_{90} = 160 °C). It is interesting to note that the ranking of CO oxidation activity on Pt/CeO_2 and Pt/CZO was reversed after activation, and this was the result of different structural evolution processes during activation, leading to distinct final states of Pt species. Pt catalysts supported on $Ce_xZr_{1-x}O_2$ with different amounts of Zr dopant (x = 0.95, 0.9, 0.85, 0.6, and 0.3) were investigated, and Pt/CZO-a (Pt/$Ce_{0.9}Zr_{0.1}O_2$) was found to perform the best for CO oxidation (SI Figures S4 and S5). After aging treatment and activation, Pt/CeO_2-800A-a showed a significant activity decrease below 150 °C, whereas Pt/CZO-800A-a only showed a slight activity decline below 100 °C but an increase above 100 °C (Figure 2b). The much higher CO oxidation activity on Pt/CZO-1000A-a (T_{90} = 212 °C) than that on Pt/CeO_2-1000A-a (T_{90} = 377 °C) further supported the viewpoint that Pt/CZO exhibited superior thermal stability (SI Figure S6). The long-term stability test also suggested that Pt/CZO-800A-a could maintain relatively stable activity under the reaction conditions at low temperatures (SI Figure S7).

To further compare the defect engineered CZO with commercially available CeO_2-based supports, the CO oxidation activities on Pt catalysts supported on commercial high surface area CeO_2 and $CeZrO_x$ (i.e., Pt/CeO_2_c and Pt/CZO_c) were also evaluated (Figure 2c,d). Before the test, activation treatment by H_2 was also performed on Pt/CeO_2_c and Pt/CZO_c to promote their catalytic performance (Pt/CeO_2_c-a and Pt/CZO_c-a). Activated Pt/CZO catalyst outperformed Pt/CeO_2_c-a and Pt/CZO_c-a not only before but also after high temperature aging treatment. As previously reported, CeO_2 nanorod (CeO_2_NR) was one of the most frequently used supports for the synthesis of highly efficient Pt/CeO_2 catalysts.[25,26,59] Therefore, the CO oxidation activities on Pt/CeO_2_NR-a and Pt/CeO_2_NR-800A-a were also tested as references. The Pt/CZO-a catalyst clearly showed a much higher CO oxidation activity than Pt/CeO_2_NR-a throughout the entire temperature range, especially after high temperature aging (Figure 2d). Moreover, compared with recently reported Pt-CeO_2 based materials, Pt/CZO-a and Pt/CZO-800A-a were among the most well-performed catalysts (SI Table S4). In short, the activated Pt/CZO is an efficient low-temperature CO oxidation catalyst with satisfactory high temperature thermal stability.

3.3. Surface Structural Evolution. After H_2 reduction, the CO oxidation activities on both fresh and aged Pt/CeO_2 and Pt/CZO catalysts were greatly enhanced, indicating that a striking structural evolution of the catalytically active center occurred during the activation process. The higher CO oxidation activity on the activated Pt/CZO catalyst suggests that the resulting Pt species were more active catalytic centers relative to those on CeO_2. To better understand the change in catalyst structure, Raman spectra of Pt/CeO_2, Pt/CZO, Pt/

https://doi.org/10.1021/acs.est.1c02853
Environ. Sci. Technol. 2021, 55, 12607−12618

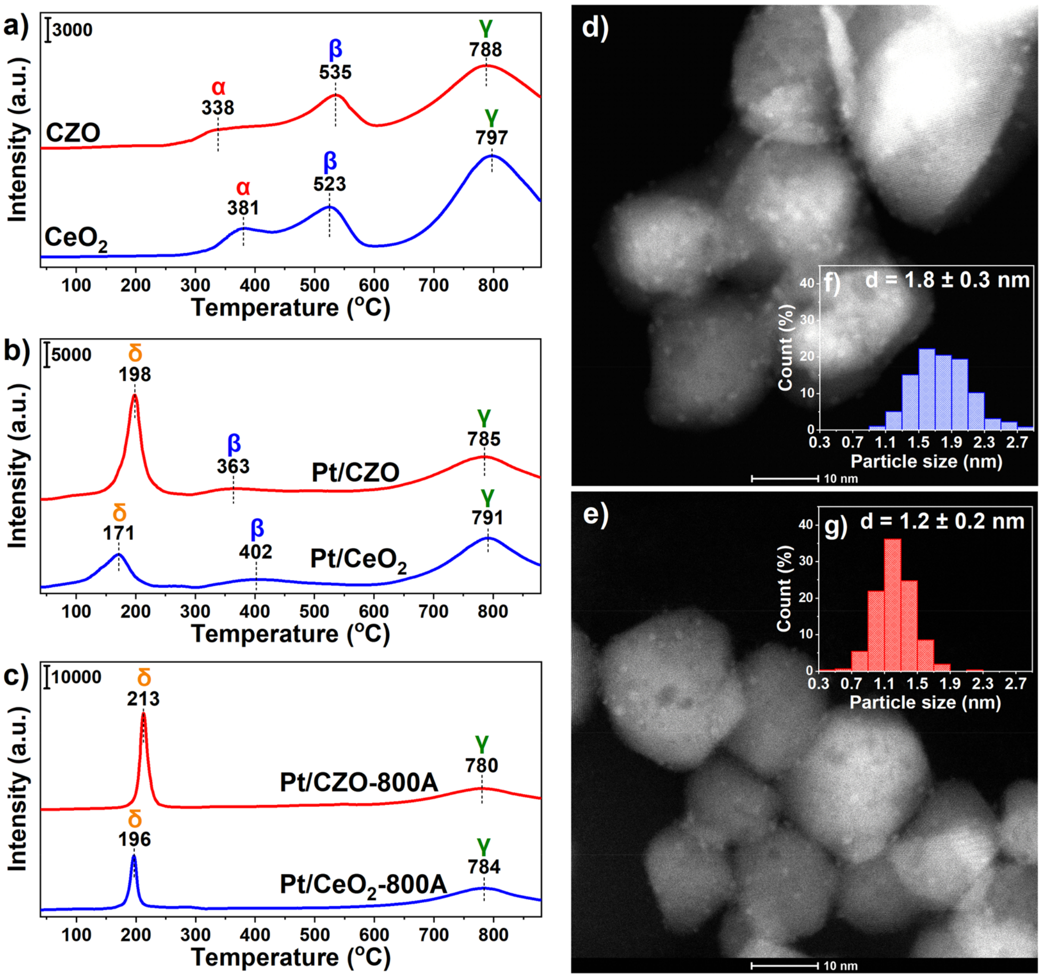

Figure 3. H_2-TPR profiles of (a) CeO_2 and CZO, (b) fresh Pt/CeO_2 and Pt/CZO, (c) aged Pt/CeO_2-800A and Pt/CZO-800A; HAADF-STEM images of (d) Pt/CeO_2-800A-a, and (e) Pt/CZO-800A-a. The Pt cluster size distributions within (f) Pt/CeO_2-800A-a and (g) Pt/CZO-800A-a were displayed in the inserted graphs (more than 300 Pt clusters were counted).

CeO_2-800A, and Pt/CZO-800A before and after activation were collected (SI Figure S8). Besides the sharp band at *ca.* 465 cm^{-1} (CeO_2 F_{2g} mode), two new bands at *ca.* 557 and 662 cm^{-1} were observed on Pt/CeO_2, Pt/CZO, Pt/CeO_2-800A and Pt/CZO-800A, which could be attributed to Pt−O−Ce and Pt−O (in Pt−O−Ce) structures.[60] The bands assigned to Pt−O−Ce and Pt−O on Pt/CZO showed higher intensity than those on Pt/CeO_2 (SI Figure S8a) for both fresh and aged samples, indicating more Pt−O−Ce linkages on Pt/CZO. After activation, the intensity of these two bands on all samples declined significantly (SI Figure S8b,c), which was related to the reduction of Pt single sites and neighboring Ce^{4+} cations. Also, as indicated by the decrease in Pt−O−Ce linkage, the Pt single sites might have agglomerated and formed Pt clusters after activation, which will be discussed later.

H_2-TPR experiment was performed to further reveal the structural evolution of Pt/CeO_2 and Pt/CZO catalysts during the activation process. Three H_2-consumption peaks were observed for CZO and CeO_2 supports (Figure 3a, SI Figure S9), where peaks α, β, and γ could be assigned to the reduction of surface oxygen species, surface Ce^{4+}, and bulk CeO_2, respectively.[46] It is interesting to note that the peak α on CZO shifted to a much lower temperature (from 381 to 338 °C) than that on CeO_2, due to the formation of more oxygen vacancies and surface adsorbed oxygen species on CZO. After Pt deposition, a new H_2-consumption peak (marked as δ) at *ca.* 180 °C was observed on both Pt/CZO and Pt/CeO_2, which could be ascribed to the reduction of Pt−O or Pt−O−Ce species (Figure 3b). For Pt/CZO, the peak δ was more intense and symmetrical, centered at a higher temperature of 198 °C (versus 171 °C on Pt/CeO_2), indicating a stronger interaction between Pt and CZO as well as more reducible oxygen species from Pt−O−Ce linkages (SI Table S5).[58,61] After aging treatment, peak δ shifted to higher temperatures and showed an increase in symmetry, indicating the stronger Pt-CeO_2 interaction on aged samples. The Pt-CeO_2 interaction on Pt/CZO-800A was still stronger than that on Pt/CeO_2-800A (Figure 3c). Based on the results of Raman spectra and H_2-TPR, higher density of surface defects and adsorbed oxygen species were created on CZO comparing to pristine CeO_2, which led to stronger Pt−O−Ce interaction on Pt/CZO and Pt/CZO-800A than that on Pt/CeO_2 and Pt/CeO_2-800A counterparts.

After activation by H_2 reduction, the less active Pt single sites transformed into active Pt species with new structures. HAADF-STEM images of Pt/CeO_2-800A-a and Pt/CZO-800A-a were collected to illustrate the state of Pt species on the activated catalysts. As shown in Figure 3d−g and SI Figure S10, abundant Pt clusters formed on Pt/CeO_2-800A-a and Pt/CZO-800A-a. The average size of Pt clusters on Pt/CZO-

https://doi.org/10.1021/acs.est.1c02853
Environ. Sci. Technol. 2021, 55, 12607−12618

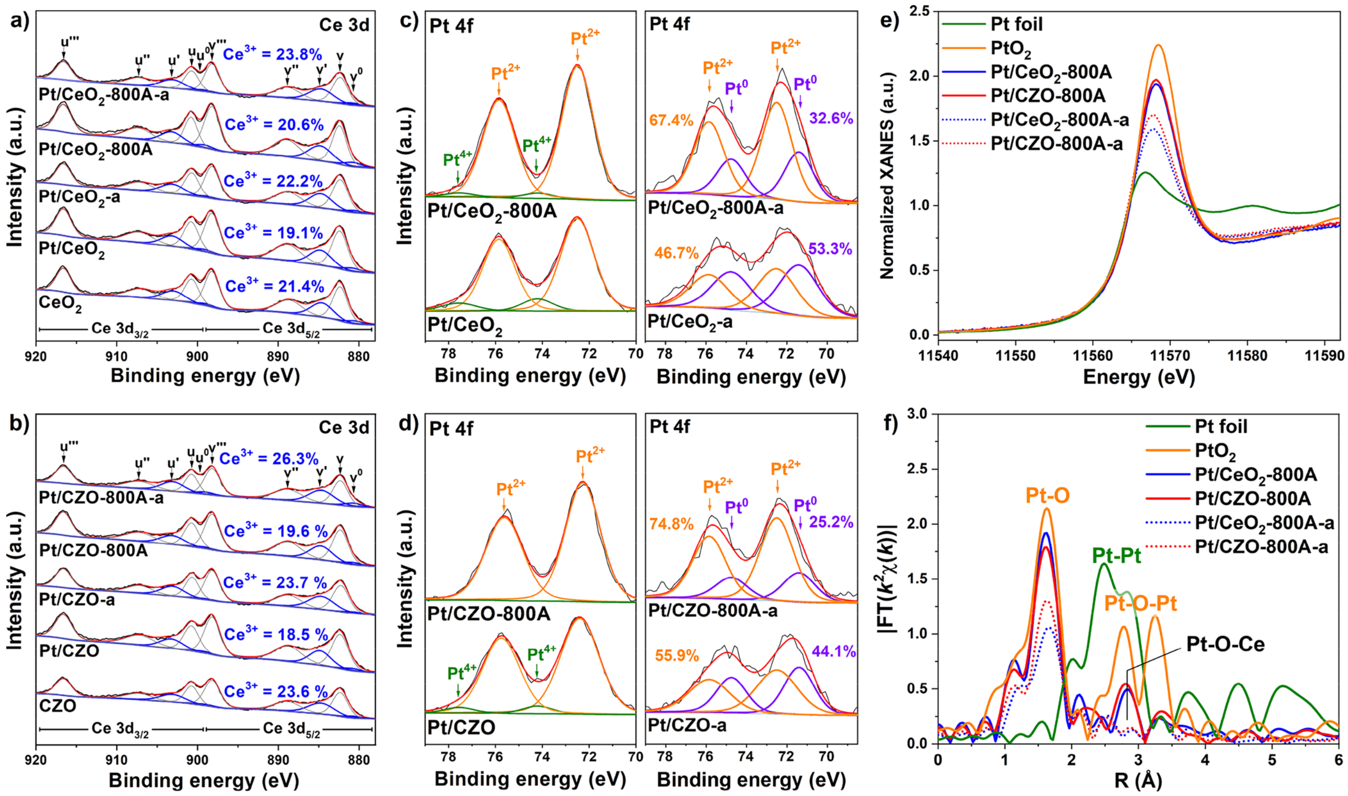

Figure 4. XPS of Ce 3d for (a) CeO_2, Pt/CeO_2, Pt/CeO_2-a, Pt/CeO_2-800A and Pt/CeO_2-800A-a; (b) CZO, Pt/CZO, Pt/CZO-a, Pt/CZO-800A and Pt/CZO-800A-a; XPS of Pt 4f for (c) Pt/CeO_2, Pt/CeO_2-800A, Pt/CeO_2-a and Pt/CeO_2-800A-a, (d) Pt/CZO, Pt/CZO-800A, Pt/CZO-a and Pt/CZO-800A-a; (e) Normalized XANES; and (f) EXAFS magnitude of the Fourier transformed k^2-weighted $\chi(k)$ data for Pt/CeO_2-800A, Pt/CZO-800A, Pt/CeO_2-800A-a, and Pt/CZO-800A-a at the Pt-L_3 edge. Reference samples of Pt foil and PtO_2 were used for comparison.

800A-a was noticeably smaller (1.2 ± 0.2 nm) than that on Pt/CeO_2-800A-a (1.8 ± 0.3 nm), and the size distribution on Pt/CZO-800A-a was narrower and more symmetric. Apparently, the more homogeneous distribution of Pt single sites and stronger Pt-CeO_2 interaction on Pt/CeZO-800A favored the formation of more uniform and much smaller Pt clusters. Interestingly, the average size of Pt clusters on Pt/CZO-800A-a (1.2 ± 0.2 nm) was very close to the optimal size of Pt clusters reported previously, where the CeO_2-supported Pt clusters with an average diameter of *ca.* 1.4 nm were just sufficiently large to efficiently activate the CeO_2 redox chemistry and provide plentiful active interfacial sites for CO oxidation.[22]

XPS measurements were carried out to characterize the surface chemical states of all the samples. The surface atomic concentration for different elements can be found in SI Table S3. As displayed in Figure 4a,b, after doping Zr^{4+} (with a smaller ionic radius, r = 0.80 Å), the concentration of surface Ce^{3+} on CeO_2 increased from 21.4% to 23.6%, a result of lattice shrinkage/strain (SI Table S1) and spontaneous transformation of Ce^{4+} (r = 0.092 nm) to Ce^{3+} (r = 0.103 nm).[62] After Pt deposition onto CeO_2 and CZO, the concentration of surface Ce^{3+} on both supports decreased, and this decrease was a result of the reaction between PtO_2 and surface Ce^{3+}, forming a strong chemical bonding of Pt^{2+}–O-Ce^{4+}.[20] After activation, the surface Ce^{3+} concentration on all activated samples showed a significant increase, especially on Pt/CZO-a and Pt/CZO-800A-a. This was in good agreement with the H_2-TPR results where the H_2 consumption peaks of Pt–O–Ce on Pt/CZO and Pt/CZO-800A were much more intense than those of Pt/CeO_2 and Pt/CeO_2-800A counterparts, suggesting the formation of more Ce^{3+} species on CZO after activation. The intensity of XRD peaks of Pt/CeO_2 and Pt/CZO reduced significantly after activation (SI Figure S11), another indication of forming more Ce^{3+} within the activated samples, which was likely to reduce the crystallinity of CeO_2 and CZO. Higher concentration of surface Ce^{3+} species is usually related to the formation of more oxygen vacancies and more abundant surface adsorbed oxygen, which is a key factor in promoting the CO oxidation activity on Pt/CZO-a and Pt/CZO-800A-a catalysts.

As shown in Figure 4c,d, Pt on fresh and aged Pt/CeO_2 and Pt/CZO was mainly in Pt^{2+} form, which was in line with previous reports that Pt single sites strongly anchored on CeO_2 tended to exist in Pt^{2+}.[19,20,55] After H_2 activation, the concentration of Pt^{2+} was reduced on both supports with the simultaneous appearance of Pt^0. Lower concentration of surface Pt^0 species was observed on Pt/CZO-a (44.1%) and Pt/CZO-800A-a (25.2%), comparing to that on Pt/CeO_2-a (53.3%) and Pt/CeO_2-800A-a (32.6%), respectively. Since all activated catalysts were exposed to air at room temperature after H_2 reduction treatment, the Pt^0 clusters formed on the activated samples, especially those located at the Pt-CeO_2 interface, are prone to be reoxidized due to their small sizes (<2 nm). The lower concentrations of Pt^0 on Pt/CZO-a and Pt/CZO-800A-a suggest that the Pt cluster sizes were smaller than the CeO_2 supported counterparts, which was well supported by the HAADF-STEM results in Figure 3.

To further reveal the structural change of Pt species during the activation treatment, XAS analysis was performed. As

https://doi.org/10.1021/acs.est.1c02853
Environ. Sci. Technol. 2021, 55, 12607−12618

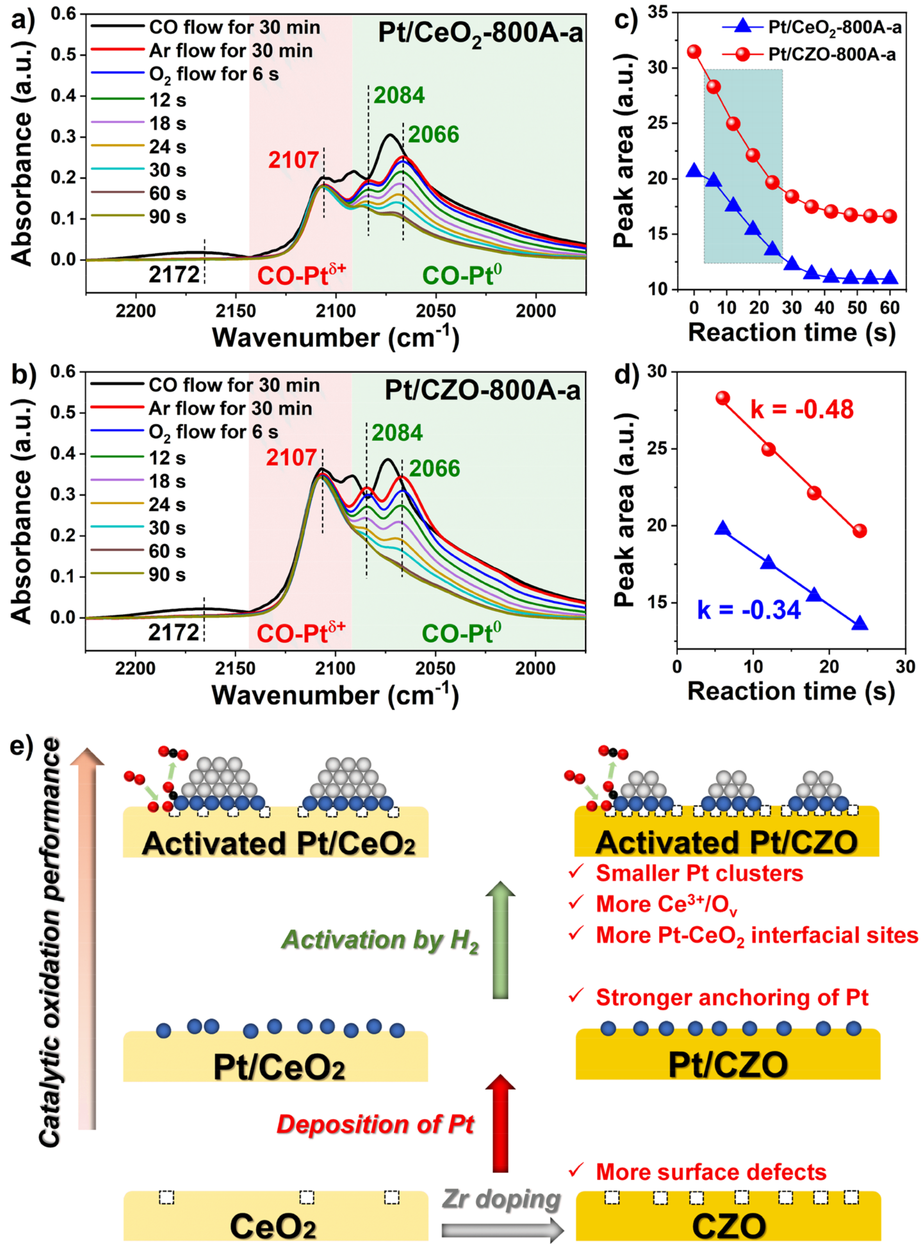

Figure 5. *In situ* DRIFTS of reaction between O_2 and preadsorbed CO on (a) Pt/CeO_2-800A-a and (b) Pt/CZO-800A-a catalysts at 50 °C; (c,d) The peak area of CO-Pt^0 as a function of reaction time (calculated based on panels a and b); (e) The structure−activity relationship of CO oxidation on Zr doped Pt/CeO_2 catalysts (Color: Pt, gray, and blue; O, red; C, black; surface defect, white square. O_v = oxygen vacancy).

shown in Figure 4e, the white line intensities of Pt-L_3 XANES for Pt/CeO_2-800A and Pt/CZO-800A were lower than that on PtO_2 but higher than that on Pt foil, indicating an intermediate valence state (between +4 and 0) of Pt on these two samples. After activation, the white line intensities obviously decreased, suggesting the lower average valence states of Pt species on activated catalysts compared to the untreated ones. Judging from the white line intensity, the valence state of Pt species on Pt/CZO-800A-a was found to be higher than that on Pt/CeO_2-800A-a, matching well with the XPS results. To further understand the local coordination structure of Pt on these catalysts before and after activation, EXAFS data were processed and plotted in R space. As shown in Figure 4f, SI Figure S12 and Table S6, the absence of Pt−Pt and Pt−O−Pt coordination shells and the existence of Pt−O and Pt−O−Ce coordination shells exclusively clearly confirm the formation of Pt single sites on Pt/CeO_2-800A and Pt/CZO-800A. The higher coordination number (CN) of Pt−O−Ce on Pt/CZO-800A (*ca.* 3.0) than that on Pt/CeO_2-800A (*ca.* 2.2) suggests that more Pt−O−Ce linkages were formed on Pt/CZO-800A, supporting the Raman spectra and H_2-TPR results. After activation, Pt/CZO-800A-a showed a lower CN of Pt−Pt (*ca.* 0.8) than Pt/CeO_2-800A-a (*ca.* 1.2), indicating again the formation of smaller Pt clusters on Pt/CZO-800A-a.[63] In agreement with the Pt 4f XPS and Pt-L_3 XANES results, the higher CN of Pt−O and Pt−O−Ce on Pt/CZO-800A-a also suggests that smaller Pt clusters, with more exposed Pt atoms, were much easier to reoxidize at the Pt-CeO_2 interface.

3.4. Identification of Active Sites. *In situ* DRIFTS of CO adsorption and oxidation on activated catalysts were performed to identify the true catalytically active sites for CO oxidation reaction. As shown in Figures 5a,b, besides the band at *ca.*

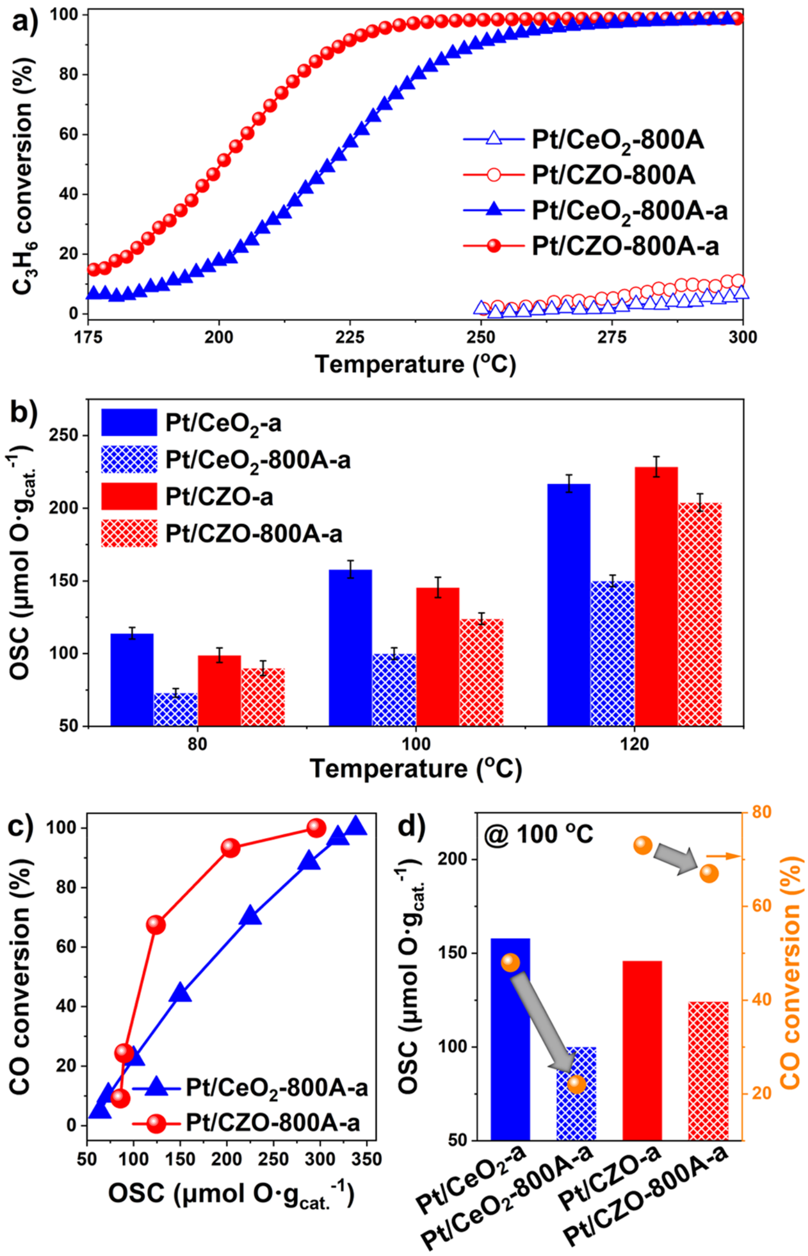

Figure 6. (a) C_3H_6 oxidation activity on Pt/CeO_2-800A and Pt/CZ0−800A that were pretreated with air at 300 °C or activated with 10% H_2 at 500 °C; (b) OSC functions on fresh and aged Pt/CeO_2 and Pt/CZO catalysts tested at different temperatures; (c) The relationship between CO conversion and OSC functions on Pt/CeO_2-800A-a and Pt/CZO-800A-a; (d) OSC functions and CO conversions at 100 °C on fresh and aged Pt/CeO_2 and Pt/CZO catalysts (all samples were activated by H_2 at 400 °C for 1 h before OSC testing).

2107 cm^{-1} assigned to CO adsorbed on PtO_x species (CO-$Pt^{\delta+}$@PtO_x), the band at *ca.* 2084 cm^{-1} attributed to CO linearly adsorbed on the terrace of metallic Pt clusters (well-coordinated Pt sites) and the band at *ca.* 2066 cm^{-1} assigned to CO adsorbed on the step and corner sites of metallic Pt clusters (under-coordinated Pt sites) were observed on both Pt/CeO_2-800A-a and Pt/CZO-800A-a.[64−66] CO adsorbed on Pt clusters were denoted as CO-Pt^0@cluster. After Ar purge and the introduction of O_2, the intensities of the bands assigned to CO-Pt^0@cluster decreased rapidly, indicating that the CO adsorbed on Pt clusters were highly reactive at a temperature as low as 50 °C. To determine the reaction rate of CO-Pt^0@Pt clusters, the integrated peak areas of CO-Pt^0@Pt clusters are plotted as a function of time and the rates of the peak area decrease are calculated. As shown in Figures 5c,d, more CO-Pt^0@Pt clusters species were found on Pt/CZO-800A-a, and the combined consumption rate of CO-Pt^0@Pt clusters on Pt/CZO-800A-a (0.48 unit/min) was much higher than that on Pt/CeO_2-800A-a (0.34 unit/min), another indication that more Pt^0 sites with higher activity were formed on Pt/CZO-800A-a.

The role of PGMs cluster-support interface in CO oxidation has been highlighted in literature, where the process of oxygen/charge transfer and intermediate diffusion across the interface were thought to largely determine the catalytic activity.[67] Cargnello *et al.* concluded that CO oxidation was highly active on the metal-CeO_2 interfacial sites for CeO_2 supported VIII metal catalysts, including Ni, Pd, Pt supported on CeO_2.[68] Liu *et al.* and Lu *et al.* also found that the Pt-CeO_2 interface was the true active site for CO oxidation, on which the activated oxygen species could react with the CO adsorbed on Pt clusters effectively.[69,70] Combining the results of HAADF-STEM, H_2-TPR, Raman spectra, XAS and *in situ* DRIFTS with the catalytic activity results from this study, we can establish a clear structure−activity relationship for CO oxidation on Zr doped Pt/CeO_2 catalyst (Figure 5e). Through H_2 activation of the strongly anchored Pt single sites within the Pt−O−Ce linkages on the defect engineered CZO support, higher density of surface Ce^{3+} species and oxygen vacancies (O_v) along with smaller Pt clusters could be obtained on Pt/CZO. The enriched Pt clusters-CeO_2 perimeter sites, assisted by the abundant Ce^{3+} and oxygen vacancies, were beneficial for the activation and transfer of active oxygen on activated Pt/CZO, thus significantly contributing to its excellent CO oxidation activity.

3.5. Catalytic Performance for C_3H_6 Oxidation and OSC Testing. To assess the hydrocarbon oxidation activities on Pt/CeO_2-800A and Pt/CZO-800A, C_3H_6 oxidation was chosen as a probe reaction, and their activities are shown in Figure 6a. Similar to CO oxidation, both Pt/CeO_2-800A and Pt/CZO-800A showed limited C_3H_6 oxidation activity. After a H_2 activation, however, their activities were dramatically enhanced with Pt/CZO-800A-a (T_{90} = 223 °C) being significantly more active than Pt/CeO_2-800A-a (T_{90} = 249 °C). C_3H_6 oxidation activity on fresh Pt/CeO_2 and Pt/CZO showed a similar trend (SI Figure S13). The superior C_3H_6 oxidation activity observed on this newly developed Pt/CZO catalyst represents a significant improvement in catalytic hydrocarbon combustion and provides a promising lead for the practical application in vehicle emission controls.

Oxygen storage capacity (OSC) is one of the most important performance indicators of automotive catalysts. To reveal the impact of Zr doping on the OSC function of the Pt/CeO_2 catalysts, the dynamic OSC of as-prepared and aged Pt/CZO and Pt/CeO_2 were tested (all catalysts were activated by H_2 at 400 °C for 1 h before testing). As shown in Figure 6b, the OSC values on fresh Pt/CeO_2-a and Pt/CZO-a were about the same. However, after aging the OSC value on Pt/CZO-800A-a was much higher than that on Pt/CeO_2-800A-a. In addition, at a given OSC value, the CO conversion was much higher on Pt/CZO-a and Pt/CZO-800A-a than on Pt/CeO_2-a and Pt/CeO_2-800A-a, respectively (Figure 6c and SI Figure S14). The robust Pt clusters on CZO support, with smaller size and more Pt-CeO_2 interface, facilitated the adsorption, activation and oxidation of CO and consequently contributed to the higher CO oxidation activity on Pt/CZO-a and Pt/CZO-800A-a, which was well supported by the results of DRIFTS study (Figure 5). Comparing to Pt/CeO_2-a, aging had a much lower impact on Pt/CZO-a in OSC function because Zr doping significantly promoted the thermal stability of Pt/CeO_2 (Figure 6d). The drastic decline in the OSC function of Pt/CeO_2-a after aging treatment could be one of the causes for the significant decrease in CO oxidation activity in the low-temperature range (<120 °C). The superior catalytic oxidation activity and more thermally stable OSC functions make the activated Pt/CZO a promising candidate as an efficient vehicle emission control catalyst.

In summary, an efficient Pt/$CeZrO_x$ (Pt/CZO) catalyst for catalytic oxidation of CO and C_3H_6 at low temperature was designed and systemically studied. Through a facile ZrO_2 doping method, more surface defects and Ce^{3+} species were created on CZO support, which promoted the formation and stabilization of Pt single sites with much stronger Pt-CeO_2 interaction than that on pristine CeO_2. Although the strongly anchored Pt single sites showed limited CO/C_3H_6 oxidation activity, after activation by H_2 reduction, superior CO/C_3H_6 oxidation activity was achieved on activated Pt/CZO catalysts, outperforming the state-of-the-art Pt/CeO_2 catalysts. It was concluded that much smaller Pt clusters could be formed on activated Pt/CZO catalysts, with more exposed Pt sites for CO adsorption and more abundant perimeter Pt cluster-CeO_2 active sites. After high-temperature aging, no obvious decline in CO/C_3H_6 oxidation activity and OSC function were observed on activated Pt/CZO, indicating the excellent thermal stability of this newly developed catalyst. This work provides a facile but efficient strategy for fabricating a robust Pt cluster oxidation catalyst using strongly anchored Pt single sites on defect engineered CeO_2-based support, and such an engineered catalyst may lead to improved catalyst technologies for vehicle emission controls.

■ ASSOCIATED CONTENT

Supporting Information

The Supporting Information is available free of charge at https://pubs.acs.org/doi/10.1021/acs.est.1c02853.

XRD, EDS-mapping, Raman spectra, CO oxidation activity on Pt/$Ce_xZr_{1-x}O_2$-a, HAADF-STEM images, XANES linear combination fitting results, EXAFS fitting curves in R-space, C_3H_6 oxidation activity, *etc.* (PDF)

■ AUTHOR INFORMATION

Corresponding Authors

Fei Gao − *Key Laboratory of Mesoscopic Chemistry of MOE, School of Chemistry and Chemical Engineering, Jiangsu Key Laboratory of Vehicle Emissions Control, School of Environment, Center of Modern Analysis, Nanjing University, Nanjing 210093, P. R. China;* orcid.org/0000-0001-8626-5509; Email: gaofei@nju.edu.cn

Fudong Liu − *Department of Civil, Environmental, and Construction Engineering, Catalysis Cluster for Renewable Energy and Chemical Transformations (REACT), NanoScience Technology Center (NSTC), University of Central Florida, Orlando, Florida 32816, United States;* orcid.org/0000-0001-8771-5938; Email: fudong.liu@ucf.edu

Authors

Wei Tan − *Department of Civil, Environmental, and Construction Engineering, Catalysis Cluster for Renewable Energy and Chemical Transformations (REACT), NanoScience Technology Center (NSTC), University of Central Florida, Orlando, Florida 32816, United States; Key Laboratory of Mesoscopic Chemistry of MOE, School of Chemistry and Chemical Engineering, Jiangsu Key Laboratory of Vehicle Emissions Control, School of Environment, Center of Modern Analysis, Nanjing University, Nanjing 210093, P. R. China;* orcid.org/0000-0002-1481-9346

Shaohua Xie − *Department of Civil, Environmental, and Construction Engineering, Catalysis Cluster for Renewable Energy and Chemical Transformations (REACT), NanoScience Technology Center (NSTC), University of Central Florida, Orlando, Florida 32816, United States;* orcid.org/0000-0003-1550-7421

Yandi Cai — *Key Laboratory of Mesoscopic Chemistry of MOE, School of Chemistry and Chemical Engineering, Jiangsu Key Laboratory of Vehicle Emissions Control, School of Environment, Center of Modern Analysis, Nanjing University, Nanjing 210093, P. R. China*

Meiyu Wang — *College of Engineering and Applied Sciences, Nanjing University, Nanjing 210093, P. R. China*

Shuohan Yu — *Key Laboratory of Mesoscopic Chemistry of MOE, School of Chemistry and Chemical Engineering, Jiangsu Key Laboratory of Vehicle Emissions Control, School of Environment, Center of Modern Analysis, Nanjing University, Nanjing 210093, P. R. China*

Ke-Bin Low — *BASF Corporation, Iselin, New Jersey 08830, United States*

Yuejin Li — *BASF Corporation, Iselin, New Jersey 08830, United States*

Lu Ma — *National Synchrotron Light Source II (NSLS-II), Brookhaven National Laboratory, Upton, New York 11973, United States*

Steven N. Ehrlich — *National Synchrotron Light Source II (NSLS-II), Brookhaven National Laboratory, Upton, New York 11973, United States*

Lin Dong — *Key Laboratory of Mesoscopic Chemistry of MOE, School of Chemistry and Chemical Engineering, Jiangsu Key Laboratory of Vehicle Emissions Control, School of Environment, Center of Modern Analysis, Nanjing University, Nanjing 210093, P. R. China;* orcid.org/0000-0002-8393-6669

Complete contact information is available at: https://pubs.acs.org/10.1021/acs.est.1c02853

Author Contributions

The manuscript was written through the contributions from all authors. All authors have given approval to the final version of the manuscript.

Notes

The authors declare no competing financial interest.

■ ACKNOWLEDGMENTS

F.L. acknowledges Startup Fund from the University of Central Florida (UCF). S.X. thanks the support from the Preeminent Postdoctoral Program (P3) at UCF. F.G. acknowledges the support from the National Natural Science Foundation of China (No. 21972063) and Natural Science Foundation of Jiangsu Province (BK20200012). F.L. sincerely thanks Mrs. Hiroshi Kodama and Sho Hasegawa at Daiichi Kigenso Kagaku Kogyo Co., Ltd. for providing raw materials in catalyst synthesis. This research used beamline 7-BM (QAS) of the National Synchrotron Light Source II, a U.S. Department of Energy (DOE) Office of Science User Facility operated for the DOE Office of Science by Brookhaven National Laboratory under Contract No. DE-SC0012704.

■ REFERENCES

(1) Datye, A.K.; Votsmeier, M. Opportunities and Challenges in the Development of Advanced Materials for Emission Control Catalysts. *Nat. Mater.* **2021**, *20*, 1049−1059.

(2) Price Pressures on Metals, *Nat. Catal.*, **2019**,*2*, 735−735. DOI: 10.1038/s41929-019-0359-7.

(3) Bera, P.; Patil, K.; Jayaram, V.; Subbanna, G.; Hegde, M. Ionic Dispersion of Pt and Pd on CeO_2 by Combustion Method: Effect of Metal-Ceria Interaction on Catalytic Activities for NO Reduction and CO and Hydrocarbon Oxidation. *J. Catal.* **2000**, *196*, 293−301.

(4) Niishiro, R.; Kato, H.; Kudo, A. Nickel and either Tantalum or Niobium-Codoped Ti O_2 and $SrTiO_3$ Photocatalysts with Visible-Light Response for H_2 or O_2 Evolution from Aqueous Solutions. *Phys. Chem. Chem. Phys.* **2005**, *7*, 2241−2245.

(5) Kong, L.; Wang, C.; Zheng, H.; Zhang, X.; Liu, Y. Defect-Induced Yellow Color in Nb-Doped Ti O_2 and Its Impact on Visible-Light Photocatalysis. *J. Phys. Chem. C* **2015**, *119*, 16623−16632.

(6) Carrettin, S.; Hao, Y.; Aguilar-Guerrero, V.; Gates, B. C.; Trasobares, S.; Calvino, J. J.; Corma, A. Increasing the Number of Oxygen Vacancies on TiO_2 by Doping with Iron Increases the Activity of Supported Gold for CO Oxidation. *Chem. - Eur. J.* **2007**, *13*, 7771−7779.

(7) Wang, C.; Li, Y.; Zhang, C.; Chen, X.; Liu, C.; Weng, W.; Shan, W.; He, H. A Simple Strategy to Improve Pd Dispersion and Enhance Pd/TiO_2 Catalytic Activity for Formaldehyde Oxidation: The Roles of Surface Defects. *Appl. Catal., B* **2021**, *282*, 119540.

(8) Xiao, Q.; Wang, Y.; Zhao, Z.-J.; Pei, C.; Chen, S.; Gao, L.; Mu, R.; Fu, Q.; Gong, J. Defect-Mediated Reactivity of Pt/TiO_2 Catalysts: The Different Role of Titanium and Oxygen Vacancies. *Sci. China: Chem.* **2020**, *63*, 1323−1330.

(9) Wan, J.; Chen, W.; Jia, C.; Zheng, L.; Dong, J.; Zheng, X.; Wang, Y.; Yan, W.; Chen, C.; Peng, Q.; Wang, D.; Li, Y. Defect Effects on TiO_2 Nanosheets: Stabilizing Single Atomic Site Au and Promoting Catalytic Properties. *Adv. Mater.* **2018**, *30*, 1705369.

(10) Jiang, Z.; Qi, R.; Huang, Z.; Shangguan, W.; Wong, R. J.; Lee, A. Impact of Methanol Photomediated Surface Defects on Photocatalytic H_2 Production Over Pt/TiO_2. *Energy Environ. Mater.* **2020**, *3*, 202−208.

(11) Liu, M.-H.; Chen, Y.-W.; Lin, T.-S.; Mou, C.-Y. Defective Mesocrystal ZnO-Supported Gold Catalysts: Facilitating CO Oxidation via Vacancy Defects in ZnO. *ACS Catal.* **2018**, *8*, 6862−6869.

(12) Liu, M.-H.; Chen, Y.-W.; Liu, X.; Kuo, J.-L.; Chu, M.-W.; Mou, C.-Y. Defect-Mediated Gold Substitution Doping in ZnO Mesocrystals and Catalysis in CO Oxidation. *ACS Catal.* **2016**, *6*, 115−122.

(13) Feng, B.; Shi, M.; Liu, J.; Han, X.; Lan, Z.; Gu, H.; Wang, X.; Sun, H.; Zhang, Q.; Li, H.; Wang, Y.; Li, H. An Efficient Defect Engineering Strategy to Enhance Catalytic Performances of Co_3O_4 Nanorods for CO Oxidation. *J. Hazard. Mater.* **2020**, *394*, 122540.

(14) Tran, S. B. T.; Choi, H.; Oh, S.; Park, J. Y. Defective Nb_2O_5-Supported Pt Catalysts for CO Oxidation: Promoting Catalytic Activity via Oxygen Vacancy Engineering. *J. Catal.* **2019**, *375*, 124−134.

(15) Yu, Q.; Liu, C.; Li, X.; Wang, C.; Wang, X.; Cao, H.; Zhao, M.; Wu, G.; Su, W.; Ma, T.; Zhang, J.; Bao, H.; Wang, J.; Ding, B.; He, M.; Yamauchi, Y.; Zhao, X. S. N-Doping Activated Defective Co3O4 as an Efficient Catalyst for Low-Temperature Methane Oxidation. *Appl. Catal., B* **2020**, *269*, 118757.

(16) Pereira-Hernández, X. I.; DeLaRiva, A.; Muravev, V.; Kunwar, D.; Xiong, H.; Sudduth, B.; Engelhard, M.; Kovarik, L.; Hensen, E. J. M.; Wang, Y.; Datye, A. K. Tuning Pt-CeO_2 Interactions by High-Temperature Vapor-Phase Synthesis for Improved Reducibility of Lattice Oxygen. *Nat. Commun.* **2019**, *10*, 1358.

(17) Tan, W.; Alsenani, H.; Xie, S.; Cai, Y.; Xu, P.; Liu, A.; Ji, J.; Gao, F.; Dong, L.; Chukwu, E.; Yang, M.; Liu, F. Tuning Single-atom Pt_1-CeO_2 Catalyst for Efficient CO and C_3H_6 Oxidation: Size Effect of Ceria on Pt Structural Evolution. *ChemNanoMat* **2020**, *6*, 1797−1805.

(18) Jeong, H.; Shin, D.; Kim, B. S.; Bae, J.; Shin, S.; Choe, C.; Han, J. W.; Lee, H. Controlling the Oxidation State of Pt Single Atoms for Maximizing Catalytic Activity. *Angew. Chem., Int. Ed.* **2020**, *59*, 20691−20696.

(19) Nie, L.; Mei, D.; Xiong, H.; Peng, B.; Ren, Z.; Hernandez, X. I. P.; DeLaRiva, A.; Wang, M.; Engelhard, M. H.; Kovarik, L. Activation of Surface Lattice Oxygen in Single-Atom Pt/CeO_2 for Low-Temperature CO Oxidation. *Science* **2017**, *358*, 1419−1423.

(20) Kunwar, D.; Zhou, S.; DeLaRiva, A.; Peterson, E. J.; Xiong, H.; Pereira-Hernández, X. I.; Purdy, S. C.; ter Veen, R.; Brongersma, H. H.; Miller, J. T.; Hashiguchi, H.; Kovarik, L.; Lin, S.; Guo, H.; Wang,

Y.; Datye, A. K. Stabilizing High Metal Loadings of Thermally Stable Platinum Single Atoms on an Industrial Catalyst Support. *ACS Catal.* **2019**, *9*, 3978−3990.

(21) Wang, H.; Liu, J.-X.; Allard, L. F.; Lee, S.; Liu, J.; Li, H.; Wang, J.; Wang, J.; Oh, S. H.; Li, W.; Flytzani-Stephanopoulos, M.; Shen, M.; Goldsmith, B. R.; Yang, M. Surpassing the Single-Atom Catalytic Activity Limit through Paired Pt-O-Pt Ensemble Built from Isolated Pt_1 Atoms. *Nat. Commun.* **2019**, *10*, 3808.

(22) Gänzler, A. M.; Casapu, M.; Maurer, F.; Störmer, H.; Gerthsen, D.; Ferré, G.; Vernoux, P.; Bornmann, B.; Frahm, R.; Murzin, V.; Nachtegaal, M.; Votsmeier, M.; Grunwaldt, J.-D. Tuning the Pt/CeO_2 Interface by *In Situ* Variation of the Pt Particle Size. *ACS Catal.* **2018**, *8*, 4800−4811.

(23) Dvořák, F.; Camellone, M. F.; Tovt, A.; Tran, N.-D.; Negreiros, F. R.; Vorokhta, M.; Skála, T.; Matolínová, I.; Mysliveček, J.; Matolín, V. Creating Single-Atom Pt-Ceria Catalysts by Surface Step Decoration. *Nat. Commun.* **2016**, *7*, 10801.

(24) Jones, J.; Xiong, H.; DeLaRiva, A. T.; Peterson, E. J.; Pham, H.; Challa, S. R.; Qi, G.; Oh, S.; Wiebenga, M. H.; Hernández, X. I. P. Thermally Stable Single-Atom Platinum-on-Ceria Catalysts via Atom Trapping. *Science* **2016**, *353*, 150−154.

(25) Chen, J.; Wanyan, Y.; Zeng, J.; Fang, H.; Li, Z.; Dong, Y.; Qin, R.; Wu, C.; Liu, D.; Wang, M.; Kuang, Q.; Xie, Z.; Zheng, L. Surface Engineering Protocol To Obtain an Atomically Dispersed Pt/CeO_2 Catalyst with High Activity and Stability for CO Oxidation. *ACS Sustainable Chem. Eng.* **2018**, *6*, 14054−14062.

(26) Li, J.; Tang, Y.; Ma, Y.; Zhang, Z.; Tao, F.; Qu, Y. *In Situ* Formation of Isolated Bimetallic PtCe Sites of Single-Dispersed Pt on CeO_2 for Low-Temperature CO Oxidation. *ACS Appl. Mater. Interfaces* **2018**, *10*, 38134−38140.

(27) Wang, C.; Mao, S.; Wang, Z.; Chen, Y.; Yuan, W.; Ou, Y.; Zhang, H.; Gong, Y.; Wang, Y.; Mei, B.; Jiang, Z.; Wang, Y. Insight into Single-Atom-Induced Unconventional Size Dependence over CeO_2-Supported Pt Catalysts. *Chem.* **2020**, *6*, 752−765.

(28) Tao, L.; Shi, Y.; Huang, Y.-C.; Chen, R.; Zhang, Y.; Huo, J.; Zou, Y.; Yu, G.; Luo, J.; Dong, C.-L.; Wang, S. Interface Engineering of Pt and CeO_2 Nanorods with Unique Interaction for Methanol Oxidation. *Nano Energy* **2018**, *53*, 604−612.

(29) Kunwar, D.; Zhou, S.; DeLaRiva, A.; Peterson, E. J.; Xiong, H.; Pereira-Hernández, X. I.; Purdy, S. C.; ter Veen, R.; Brongersma, H. H.; Miller, J. T. Stabilizing High Metal Loadings of Thermally Stable Platinum Single Atoms on an Industrial Catalyst Support. *ACS Catal.* **2019**, *9*, 3978−3990.

(30) Jeong, H.; Kwon, O.; Kim, B.-S.; Bae, J.; Shin, S.; Kim, H.-E.; Kim, J.; Lee, H. Highly Durable Metal Ensemble Catalysts with Full Dispersion for Automotive Applications Beyond Single-Atom Catalysts. *Nat. Catal.* **2020**, *3*, 368−375.

(31) Trovarelli, A.; Boaro, M.; Rocchini, E.; de Leitenburg, C.; Dolcetti, G. Some Recent Developments in the Characterization of Ceria-Based Catalysts. *J. Alloys Compd.* **2001**, *323*, 584−591.

(32) Trovarelli, A. Catalytic Properties of Ceria and CeO_2-Containing Materials. *Catal. Rev.: Sci. Eng.* **1996**, *38*, 439−520.

(33) Reddy, B. M.; Khan, A. Nanosized CeO_2-SiO_2, CeO_2-TiO_2, and CeO_2-ZrO_2 Mixed Oxides: Influence of Supporting Oxide on Thermal Stability and Oxygen Storage Properties of Ceria. *Catal. Surv. Asia* **2005**, *9*, 155−171.

(34) Alcala, R.; DeLaRiva, A.; Peterson, E. J.; Benavidez, A.; Garcia-Vargas, C. E.; Jiang, D.; Pereira-Hernández, X. I.; Brongersma, H. H.; Veen, R.t.; Staněk, J.; Miller, J. T.; Wang, Y.; Datye, A. Atomically Dispersed Dopants for Stabilizing Ceria Surface Area. *Appl. Catal., B* **2021**, *284*, 119722.

(35) Xiao, Z.; Li, Y.; Hou, F.; Wu, C.; Pan, L.; Zou, J.; Wang, L.; Zhang, X.; Liu, G.; Li, G. Engineering Oxygen Vacancies and Nickel Dispersion on CeO_2 by Pr Doping for Highly Stable Ethanol Steam Reforming. *Appl. Catal., B* **2019**, *258*, 117940.

(36) Ozawa, M.; Kimura, M.; Isogai, A. The Application of Ce-Zr Oxide Solid Solution to Oxygen Storage Promoters in Automotive Catalysts. *J. Alloys Compd.* **1993**, *193*, 73−75.

(37) Rangaswamy, A.; Sudarsanam, P.; Reddy, B. M. Rare Earth Metal Doped CeO_2-Based Catalytic Materials for Diesel Soot Oxidation at Lower Temperatures. *J. Rare Earths* **2015**, *33*, 1162−1169.

(38) Liu, Z.; Yi, Y.; Zhang, S.; Zhu, T.; Zhu, J.; Wang, J. Selective Catalytic Reduction of NO_x with NH_3 over Mn-Ce Mixed Oxide Catalyst at Low Temperatures. *Catal. Today* **2013**, *216*, 76−81.

(39) Reddy, B. M.; Khan, A.; Lakshmanan, P.; Aouine, M.; Loridant, S.; Volta, J. C. Structural Characterization of Nanosized CeO_2-SiO_2, CeO_2-TiO_2, and CeO_2-ZrO_2 Catalysts by XRD, Raman, and HREM Techniques. *J. Phys. Chem. B* **2005**, *109*, 3355−3363.

(40) Dong, C.; Zong, X.; Jiang, W.; Niu, L.; Liu, Z.; Qu, D.; Wang, X.; Sun, Z. Recent Advances of Ceria-Based Materials in the Oxidation of Carbon Monoxide. *Small Struct.* **2021**, *2*, 2000081.

(41) Singhania, A. High Surface Area M (M = La, Pr, Nd, and Pm)-Doped Ceria Nanoparticles: Synthesis, Characterization, and Activity Comparison for CO Oxidation. *Ind. Eng. Chem. Res.* **2017**, *56*, 13594−13601.

(42) Han, L.; Cai, S.; Gao, M.; Hasegawa, J.-y.; Wang, P.; Zhang, J.; Shi, L.; Zhang, D. Selective Catalytic Reduction of NO x with NH3 by Using Novel Catalysts: State of the Art and Future Prospects. *Chem. Rev.* **2019**, *119*, 10916−10976.

(43) Fornasiero, P.; Montini, T.; Melchionna, M.; Monai, M. Fundamentals and Catalytic Applications of CeO_2-Based Materials. *Chem. Rev.* **2016**, *116*, 5987−6041.

(44) Kapar, J.; Fornasiero, P.; Graziani, M. Use of CeO_2-Based Oxides in the Three-way Catalysis. *Catal. Today* **1999**, *50*, 285−298.

(45) Devaiah, D.; Reddy, L. H.; Park, S.-E.; Reddy, B. M. Ceria-Zirconia Mixed Oxides: Synthetic Methods and Applications. *Catal. Rev.: Sci. Eng.* **2018**, *60*, 177−277.

(46) Tan, W.; Wang, J.; Li, L.; Liu, A.; Song, G.; Guo, K.; Luo, Y.; Liu, F.; Gao, F.; Dong, L. Gas Phase Sulfation of Ceria-Zirconia Solid Solutions for Generating Highly Efficient and SO_2 Resistant NH_3-SCR Catalysts for NO Removal. *J. Hazard. Mater.* **2020**, *388*, 121729.

(47) Lang, W.; Laing, P.; Cheng, Y.; Hubbard, C.; Harold, M. P. Co-Oxidation of CO and Propylene on Pd/CeO_2-ZrO_2 and Pd/Al_2O_3 Monolith Catalysts: A Light-off, Kinetics, and Mechanistic Study. *Appl. Catal., B* **2017**, *218*, 430−442.

(48) Yang, X.; Cheng, X.; Ma, J.; Zou, Y.; Luo, W.; Deng, Y. Large-Pore Mesoporous CeO_2-ZrO_2 Solid Solutions with In-Pore Confined Pt Nanoparticles for Enhanced CO Oxidation. *Small* **2019**, *15*, 1903058.

(49) Zheng, Y.; Li, K.; Wang, H.; Wang, Y.; Tian, D.; Wei, Y.; Zhu, X.; Zeng, C.; Luo, Y. Structure Dependence and Reaction Mechanism of CO Oxidation: A Model Study on Macroporous CeO_2 and CeO_2-ZrO_2 Catalysts. *J. Catal.* **2016**, *344*, 365−377.

(50) Li, H.; Shen, M.; Wang, J.; Wang, H.; Wang, J. Effect of Support on CO Oxidation Performance over the Pd/CeO_2 and Pd/CeO_2-ZrO_2 Catalyst. *Ind. Eng. Chem. Res.* **2020**, *59*, 1477−1486.

(51) Liu, L.; Yao, Z.; Liu, B.; Dong, L. Correlation of Structural Characteristics with Catalytic Performance of CuO/$Ce_xZr_{1-x}O_2$ Catalysts for NO Reduction by CO. *J. Catal.* **2010**, *275*, 45−60.

(52) Loridant, S. Raman Spectroscopy as a Powerful Tool to Characterize Ceria-Based Catalysts, *Catal. Today*, **2021**. 37398.

(53) Wu, Z.; Li, M.; Mullins, D. R.; Overbury, S. H. Probing the Surface Sites of CeO_2 Nanocrystals with Well-Defined Surface Planes via Methanol Adsorption and Desorption. *ACS Catal.* **2012**, *2*, 2224−2234.

(54) Li, J.; Guan, Q.; Wu, H.; Liu, W.; Lin, Y.; Sun, Z.; Ye, X.; Zheng, X.; Pan, H.; Zhu, J.; Chen, S.; Zhang, W.; Wei, S.; Lu, J. Highly Active and Stable Metal Single-Atom Catalysts Achieved by Strong Electronic Metal-Support Interactions. *J. Am. Chem. Soc.* **2019**, *141*, 14515−14519.

(55) Ye, X.; Wang, H.; Lin, Y.; Liu, X.; Cao, L.; Gu, J.; Lu, J. Insight of the Stability and Activity of Platinum Single Atoms on Ceria. *Nano Res.* **2019**, *12*, 1401−1409.

(56) Fan, L.; Wang, K.; Xu, K.; Liang, Z.; Wang, H.; Zhou, S.-F.; Zhan, G. Structural Isomerism of Two Ce-BTC for Fabricating Pt/

CeO_2 Nanorods toward Low-Temperature CO Oxidation. *Small* **2020**, *16*, 2003597.
(57) Li, J.; Guan, Q.; Wu, H.; Liu, W.; Lin, Y.; Sun, Z.; Ye, X.; Zheng, X.; Pan, H.; Zhu, J.; Chen, S.; Zhang, W.; Wei, S.; Lu, J. Highly Active and Stable Metal Single-Atom Catalysts Achieved by Strong Electronic Metal-Support Interactions. *J. Am. Chem. Soc.* **2019**, *141*, 14515−14519.
(58) Lee, J.; Ryou, Y.; Chan, X.; Kim, T. J.; Kim, D. H. How Pt Interacts with CeO_2 under the Reducing and Oxidizing Environments at Elevated Temperature: The Origin of Improved Thermal Stability of Pt/CeO_2 Compared to CeO_2. *J. Phys. Chem. C* **2016**, *120*, 25870−25879.
(59) Cao, F.; Zhang, S.; Gao, W.; Cao, T.; Qu, Y. Facile Synthesis of Highly-Dispersed Pt/CeO_2 by a Spontaneous Surface Redox Chemical Reaction for CO Oxidation. *Catal. Sci. Technol.* **2018**, *8*, 3233−3237.
(60) Brogan, M. S.; Dines, T. J.; Cairns, J. A. Raman Spectroscopic Study of the Pt-CeO_2 Interaction in the Pt/Al_2O_3-CeO_2 Catalyst. *J. Chem. Soc., Faraday Trans.* **1994**, *90*, 1461−1466.
(61) Gao, Y.; Wang, W.; Chang, S.; Huang, W. Morphology Effect of CeO_2 Support in the Preparation, Metal-Support Interaction, and Catalytic Performance of Pt/CeO_2 Catalysts. *ChemCatChem* **2013**, *5*, 3610−3620.
(62) Yao, X.; Tang, C.; Ji, Z.; Dai, Y.; Cao, Y.; Gao, F.; Dong, L.; Chen, Y. Investigation of the Physicochemical Properties and Catalytic Activities of $Ce_{0.67}M_{0.33}O_2$ (M = Zr^{4+}, Ti^{4+}, Sn^{4+}) Solid Solutions for NO Removal by CO. *Catal. Sci. Technol.* **2013**, *3*, 688−698.
(63) Liu, A.; Liu, X.; Liu, L.; Pu, Y.; Guo, K.; Tan, W.; Gao, S.; Luo, Y.; Yu, S.; Si, R. Getting Insights into the Temperature-Specific Active Sites on Platinum Nanoparticles for CO Oxidation: A Combined *in Situ* Spectroscopic and ab Initio Density Functional Theory Study. *ACS Catal.* **2019**, *9*, 7759−7768.
(64) Avanesian, T.; Dai, S.; Kale, M. J.; Graham, G. W.; Pan, X.; Christopher, P. Quantitative and Atomic-Scale View of CO-Induced Pt Nanoparticle Surface Reconstruction at Saturation Coverage via DFT Calculations Coupled with *in Situ* TEM and IR. *J. Am. Chem. Soc.* **2017**, *139*, 4551−4558.
(65) Pozdnyakova, O.; Teschner, D.; Wootsch, A.; Kröhnert, J.; Steinhauer, B.; Sauer, H.; Toth, L.; Jentoft, F. C.; Knop-Gericke, A.; Paál, Z.; Schlögl, R. Preferential CO Oxidation in Hydrogen (PROX) on Ceria-Supported Catalysts, Part I: Oxidation State and Surface Species on Pt/CeO_2 under Reaction Conditions. *J. Catal.* **2006**, *237*, 1−16.
(66) Ding, K.; Gulec, A.; Johnson, A. M.; Schweitzer, N. M.; Stucky, G. D.; Marks, L. D.; Stair, P. C. Identification of Active Sites in CO Oxidation and Water-Gas Shift over Supported Pt Catalysts. *Science* **2015**, *350*, 189−192.
(67) Puigdollers, A. R.; Schlexer, P.; Tosoni, S.; Pacchioni, G. Increasing Oxide Reducibility: The Role of Metal/Oxide Interfaces in the Formation of Oxygen Vacancies. *ACS Catal.* **2017**, *7*, 6493−6513.
(68) Cargnello, M.; Doan-Nguyen, V. V.; Gordon, T. R.; Diaz, R. E.; Stach, E. A.; Gorte, R. J.; Fornasiero, P.; Murray, C. B. Control of Metal Nanocrystal Size Reveals Metal-Support Interface Role for Ceria Catalysts. *Science* **2013**, *341*, 771−773.
(69) Lu, Y.; Thompson, C.; Kunwar, D.; Datye, A. K.; Karim, A. M. Origin of the High CO Oxidation Activity on CeO_2 Supported Pt Nanoparticles: Weaker Binding of CO or Facile oxygen Transfer from the Support? *ChemCatChem* **2020**, *12*, 1726−1733.
(70) Liu, H.-H.; Wang, Y.; Jia, A.-P.; Wang, S.-Y.; Luo, M.-F.; Lu, J.-Q. Oxygen Vacancy Promoted CO Oxidation over Pt/CeO_2 Catalysts: A Reaction at Pt-CeO_2 Interface. *Appl. Surf. Sci.* **2014**, *314*, 725−734.

https://doi.org/10.1021/acs.est.1c02853
Environ. Sci. Technol. 2021, 55, 12607−12618